ResearchGate

See discussions, stats, and author profiles for this publication at: https://www.researchgate.net/publication/259284962

Influence of Phosphorus on Alkali Distribution during Combustion of Logging Residues and Wheat Straw in a Bench-Scale Fluidized Bed

ARTICLE *in* ENERGY & FUELS · MAY 2012

Impact Factor: 2.79 · DOI: 10.1021/ef300275e

CITATIONS
17

READS
69

5 AUTHORS, INCLUDING:

Alejandro Grimm
Swedish University of Agricultural Sciences
17 PUBLICATIONS **412** CITATIONS
SEE PROFILE

Nils Skoglund
Luleå University of Technology
10 PUBLICATIONS **169** CITATIONS
SEE PROFILE

Dan Boström
Umeå University
136 PUBLICATIONS **1,980** CITATIONS
SEE PROFILE

Christoffer Boman
Umeå University
82 PUBLICATIONS **1,483** CITATIONS
SEE PROFILE

Available from: Alejandro Grimm
Retrieved on: 01 February 2016

energy&fuels

Article

pubs.acs.org/EF

Influence of Phosphorus on Alkali Distribution during Combustion of Logging Residues and Wheat Straw in a Bench-Scale Fluidized Bed

Alejandro Grimm,*[,†] Nils Skoglund,[‡] Dan Boström,[‡] Christoffer Boman,[‡] and Marcus Öhman[†]

[†]Energy Engineering, Department of Engineering Sciences & Mathematics, Luleå University of Technology, SE- 971 87 Luleå, Sweden

[‡]Energy Technology and Thermal Process Chemistry, Umeå University, SE-901 87 Umeå, Sweden

ABSTRACT: The influence of phosphorus on the alkali distribution in fluidized (quartz) bed combustion using two different typical biomasses (logging residues and wheat straw) was studied. Phosphoric acid (H_3PO_4) was used as an additive. The produced ash fractions were analyzed for morphology and elemental composition by scanning electron microscopy-energy-dispersive spectroscopy (SEM-EDS), and crystalline phases by powder X-ray diffraction (P-XRD). For both fuel assortments tested, a reduction of volatilized deposit and fine particle-forming matter, containing mainly KCl, was achieved by adding phosphorus. For the wheat straw, this effect was considerable at medium and high phosphorus addition. As a consequence, an increased amount of potassium was found in the coarse ash particle fractions, principally as $CaKPO_4$, $KMgPO_4$, and $CaK_2P_2O_7$, at the same time that the levels of HCl and SO_2 in the flue gases increased. Generally, the addition of phosphorus to the studied biomasses changed the alkali distribution from being dominated by amorphous K-silicate coarse ash fractions and fine particulate KCl, to a system dominated by crystalline coarse ash of K−Ca/Mg-phosphates and fine particulate K_2SO_4. This implies that the fouling and high-temperature corrosion observed in industrial-scale combustion of problematic biofuels can possibly be reduced by employing additives rich in reactive phosphorus, on the condition that the higher concentrations of acidic gases can be tolerated. In order to achieve these effects, the relationship between alkali and alkaline-earth metals (i.e., (K + Na)/(Ca + Mg)) in the overall fuel ash must be considered. With respect to this, the formation of low-temperature-melting alkali-rich phosphates should not be promoted, to avoid potential increases in bed agglomeration tendencies and phosphorus release from the bed.

1. INTRODUCTION

As the competition for raw materials for biofuels production is expected to increase, it is most likely that new types of biofuels such as energy crops and various types of biomass waste products from the agricultural and industrial sector will be introduced into the market. Compared to woody biomasses, energy crops have a higher content of ash-forming elements, which can be up to 10 wt %.[1]

Biofuels with ash rich in alkali metals and chlorine used in biomass-fired power plants have shown a tendency to cause different alkali-related operational problems, such as fouling, bed agglomeration, and high-temperature corrosion in superheater sections, which leads to reduced installation efficiency.[2−4]

Various well-known methods to reduce alkali-related problems and protect the boiler against deposits rich in potassium and chlorine during combustion of biofuels are based on co-combustion with peat,[5−7] coal,[8,9] and sewage sludge,[10−12] or upon employing different sulfur-rich additives as well as clay minerals.[13−20]

In recent decades, most of the research work on biomass combustion, regarding alkali-related operational problems, has been focused on fuels with low phosphorus content. However, some agricultural biomasses and industrial residues, e.g., from biodiesel and cereal grain-based bioethanol production, have an ash-forming matter composition that differs from typical woody or herbaceous fuels, because of a much higher phosphorus content. Relatively few reported research works have been devoted to alkali-rich fuels/fuel mixtures with high phosphorus content, because most combustion studies concern wood-derived fuels, agricultural residues, and short-rotation energy crops where silicon, potassium, and calcium often are the main fuel ash-forming elements. The phosphorus compounds in the different phosphorus-rich fuels can either be of organic origin with a high availability and reactivity for ash transformation reactions, or of mineral origin (such as apatite in meat and bone meal fuels), which has been shown to have low reactivity.[21]

Some studies on phosphorus-rich fuels have demonstrated that phosphorus may decrease the problems related to corrosive ash deposition by converting the reactive gaseous alkali species formed during biomass combustion into high-temperature-melting alkali phosphates.[22,23] Boström et al.[22] found that the content of KCl in fine particles released during the fluidized-bed combustion of bark can be significantly reduced by mixing with phosphorus-rich biomasses. In addition, Grimm et al.[23] showed that phosphorus is the main ash element controlling the ash transformation reactions in the fluidized-bed combustion of phosphorus-rich fuels/fuel mixtures. Increasing the phosphorus content in phosphorus-poor fuels leads to the formation of bed ash dominated by phosphates instead of silicates.

Furthermore, many studies have indicated that alkaline-earth metals, principally calcium, may play an important role in the capture of potassium in K/Ca-containing phosphates.[24−28]

Received: February 15, 2012
Revised: March 31, 2012
Published: April 13, 2012

ACS Publications © 2012 American Chemical Society

dx.doi.org/10.1021/ef300275e | *Energy Fuels* 2012, 26, 3012−3023

Table 1. Total Ash Content and the Content of Main Ash-Forming Elements in the Used Fuel Assortments[a]

	Matrix I				Matrix II			
	logging residues[b]	logging residues + PA[c]	wheat straw-1[b]	wheat straw-1 + PA (low)[c]	wheat straw-2	wheat straw-2 + PA (low)[c]	wheat straw-2 + PA (medium)[c]	wheat straw-2 + PA (high)[c]
ash	2.4	2.4	5.7	5.6	6.2	6.1	6.0	5.9
Si	0.29	0.29	0.80	0.79	1.50	1.47	1.46	1.43
P	0.046	0.12	0.13	0.50	0.10	0.8	1.03	1.52
K	0.17	0.17	1.25	1.23	0.90	0.88	0.87	0.86
Na	0.014	0.014	0.03	0.03	0.03	0.03	0.03	0.03
Ca	0.51	0.50	0.40	0.40	0.46	0.45	0.45	0.44
Mg	0.061	0.06	0.10	0.10	0.08	0.078	0.078	0.076
Al	0.036	0.036	0.006	0.006	0.022	0.02	0.02	0.02
Fe	0.024	0.024	0.005	0.005	0.015	0.015	0.015	0.014
S	0.041	0.04	0.19	0.19	0.11	0.11	0.11	0.10
Cl	<0.01	<0.01	0.26	0.26	0.24	0.24	0.23	0.22
P/K[d]	0.34	0.90	0.13	0.50	0.14	1.10	1.50	2.23

[a]The values represent weight percentages of dry substance. [b]Equal to the composition of the produced pellets. [c]The values are calculated from the raw material compositions. [d]Molar ratio.

In small-scale grate combustion experiments of oat grains using different clay mineral additives, Boström et al.[24] found that, when using a kaolin additive, the proportion of condensed K-phosphates was increased at the expense of K-sulfate and KCl-rich fine-particle emissions. Higher levels of HCl and SO_2 in the flue gases were obtained as a consequence. When using calcite additive, the proportion of K-phosphate in fine-particle emissions decreased considerably, while the content of K-sulfate and KCl increased and lower levels of acidic HCl and SO_2 emissions were obtained. In similar combustion experiments with different types of cereal grains, Lindström et al.[25] showed that the addition of lime reduced or eliminated the formation of slag for all studied fuels. The effect was attributed to the formation of high-temperature-melting Ca−K-phosphates, which shows the possibilities for potassium retention in refractory ternary phosphate phases. Working with grate combustion of a phosphorus-rich fuel, Wu et al.[26] also showed that the effect of calcium-based additives greatly increased the molar ratio of K/P in flue gas ash particles. Beck and Unterberger found that in combustion experiments with high-phosphorus fuels/fuel mixtures with coal, phosphorus found in fly ash particles was primarily suggested to occur in the form of calcium phosphates.[27] In addition, Novakovic and co-authors showed that, in the K−Ca−P system, with K_2CO_3 as the K source, the Ca/P molar ratio had a strong effect on the K volatilization rate. A decreased Ca/P molar ratio (increased phosphorus content) significantly decreases the release of potassium. The authors show that potassium is preferentially incorporated in nonvolatile $(K_2O)_k(CaO)_l(P_2O_5)_m$ structures.[28]

However, the influence of phosphorus on the formation of volatile alkali compounds during fluidized (quartz)-bed combustion of phosphorus-rich biomasses is still not fully understood. Therefore, the objective of the present work was to determine the influence of phosphorus on the alkali distribution in fluidized (quartz)-bed combustion using two different biomass fuels, i.e., logging residues and wheat straw.

2. MATERIALS AND METHODS

2.1. Fuels and Additives. A total of seven different pelletized fuel assortments was produced. Logging residues from spruce harvested in northern Sweden (SCA Skog AB Norrbränslen) and two typical wheat straws from southern Sweden (i.e., straw 1 and 2) with fairly similar ash composition, were used as raw materials. Phosphoric acid (PA) (85% aqueous solution, from Merck) was selected as the additive in order to enable high reactivity and availability of the phosphorus added.

In the initial experimental matrix (part I), the following assortments were produced and combusted: (i) logging residues mixed with PA, increasing the molar ratio between phosphorus and potassium (P/K) from 0.34 to ∼0.9 and (ii) wheat straw-1 mixed with PA increasing the P/K molar ratio from 0.13 to 0.5. In addition, the experimental matrix was extended to study the effect of increased phosphorus share in the K/Si-rich wheat straw in more detail. Another wheat straw (i.e., wheat straw-2), although with a composition similar to that of straw-1, was used in these experiments, since it was not possible to obtain the same wheat straw fuel used in matrix I. Wheat straw-2 was mixed with PA on three levels, increasing the P/K molar ratio from 0.14 (reference) to 1.1 (low), 1.5 (medium), and 2.23 (high).

To obtain homogeneous mixtures, as well as good distribution and contact between the raw fuel material and the additive, the fuel/additive mixing was completed in 20-kg batches and subsequently pelletized to a diameter of 8 mm and a moisture content of 10%−12% in a laboratory-scale pellet press. Pure logging residues and wheat straw-1 were pelletized and combusted as pure fuels.

The composition of the used fuel assortments is presented in Table 1. The raw materials were analyzed for the contents of ash (SS - 18 71 71), sulfur (SS - 18 71 77), and chlorine (SS - 18 71 85), and the main ash-forming elements were determined using inductively coupled plasma−atomic emission spectroscopy (ICP-AES). The ash compositions of the produced assortments were calculated from the compositions of the raw materials.

2.2. Combustion Experiments. The fluidized-bed experiments were performed in a bench-scale bubbling fluidized-bed (BFB) reactor (5 kW) using 540 g of quartz sand (>98% SiO_2) with a grain fraction size between 200 and 250 μm as bed material. An illustration of the reactor is shown in Figure 1. The primary air flow through the distribution plate was set at 10 times the minimum fluidizing velocity (80 NL/min), corresponding to ∼1 m/s. Temperatures were measured with Type N thermocouples. A total amount of ∼5 kg of the different fuels was combusted for 8 h at an average bed temperature of 800 °C for all fuels, except for the wheat straw fuels/fuel assortments, which were combusted at an average temperature of 730 °C, to avoid fast bed defluidization. A constant temperature of ∼800 °C along the reactor was achieved via a combination of preheated primary air, heat from the fuel combustion, and electrical heaters. After the free board section, the flue gases were led through a cyclone separator with a cut size of >10 μm. During the combustion period, the flue gas temperature after the cyclone, where online flue gas analysis and

dx.doi.org/10.1021/ef300275e | Energy Fuels 2012, 26, 3012−3023

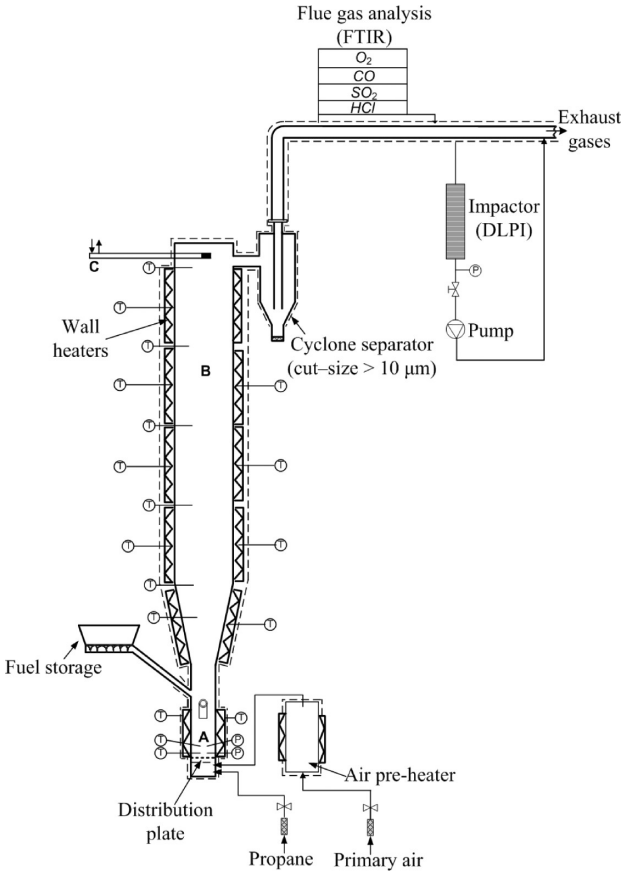

Figure 1. Illustration of the bench-scale bubbling fluidized bed (BFB) reactor and the different sampling positions: A, bed section; B, free board section; and C, air-cooled temperature-controlled deposition probe.

particulate matter sampling were measured, was 210 ± 20 °C for all experiments. The concentration of CO, SO_2, and HCl was continuously monitored during the experiments using Fourier transform infrared spectroscopy (FTIR) and the O_2 level with a lambda probe. The excess oxygen level during the experiments varied between 8% and 10% (dry basis) and the CO concentrations were <10 mg/Nm^3.

To study the alkali distribution along the system, samples of bed-, deposit-, cyclone-, and fine submicrometer-ash particles were collected. Bed material samples were taken after the combustion period, and bed ash particles were separated from the bed material grains by sieving with a 100 μm pore mesh. To study the deposit formation, an air-cooled temperature-controlled deposition probe with an exchangeable stainless steel (SS 2343) sample ring (surface area = 18 cm^2) was used, which simulates the heat exchanging surfaces of industrial biomass-fuelled boilers. The sample ring was placed in the free board section, where the flue gas temperature was ∼800 °C. The surface temperature of the probe ring was cooled to 450 °C (point C in Figure 1). The probe was inserted when stable combustion conditions were reached, i.e., after ∼1 h of combustion. The exposure time was 6 h for each combustion experiment, except for the wheat straw-2 + PA (high) assortment, which was exposed until total bed defluidization was achieved (i.e., ∼3 h).

To determine the particulate matter (PM) mass size distribution of the ash particles not trapped in the flue gas PM_{10} cyclone, isokinetic particle sampling was carried out in the flue gas channel, using a 13-step low-pressure cascade impactor from Dekati, Ltd. (DLPI), which classifies the size of ash particles according to aerodynamic diameter in the range of 0.03−10 μm. Aluminum foils (not greased) were used as substrates in the impactor, and the impactor was heated to 150 °C during the sampling.

2.3. Chemical Characterization. The chemical compositions of the formed bed ash, wind-/lee-side deposits, cyclone ash (>10 μm), and fine (<1 μm) ash particles (here, on impactor stages 4, 5, and occasionally 6, corresponding to GMD 0.19, 0.32, and 0.52 μm, respectively) were analyzed semiquantitatively, using a Philips model XL30 scanning electron microscopy (SEM) system combined with an energy-dispersive X-ray spectroscopy (EDS) device and with a powder X-ray diffraction (P-XRD) system for identification of crystalline phases.

The separated bed ash particle samples were ground (homogenized) before XRD and subsequent SEM-EDS analyses. The total amount of cyclone ash was thoroughly homogenized and a representative sample was used for XRD and SEM-EDS analyses. Prior to the SEM-EDS analysis, the samples were mounted on carbon tape and 10 area analyses (100 μm × 100 μm) were performed for these ash fractions. In addition, more than 30 individual cyclone ash particles from each experiment were analyzed in detail by SEM-EDS spot analysis. The major part of the deposits formed on the wind and lee sides of the probe rings was removed and mounted for XRD analysis. Subsequently, the samples were mounted on carbon tape and 10 SEM-EDS area analyses (100 μm × 100 μm) were performed. The impactor particle samples were removed from the aluminum plates and mounted for XRD analysis. Subsequently, the samples were mounted on carbon tape and 10 SEM-EDS area analyses (100 μm × 100 μm) were performed. The small amounts of coarse-mode ash particles (1−10 μm) sampled with the impactor did not permit analyses by either SEM or P-XRD.

The XRD data collections were performed using a Bruker d8 Advance instrument in $\theta-\theta$ mode, with an optical configuration consisting of a primary Göbel mirror, Cu Kα radiation, and a Våntec-1 detector. Continuous scans were applied. By adding repeated scans, the total data collection time for each sample lasted for at least 6 h. The PDF-2 databank,[29] together with Bruker software, was used to make initial qualitative identifications. The data were further analyzed with the Rietveld technique and crystal structure data from ICSD[30] to obtain semiquantitative information of the present crystalline phases.

3. RESULTS

3.1. Gaseous Emissions. The concentrations of HCl and SO_2 in the flue gases are shown in Table 2. Compared to the pure fuels, the levels of both HCl and SO_2 were increased when PA was used as an additive.

Table 2. HCl and SO_2 Emissions (mg/Nm^3 at 10% O_2), Given as 3-h Average Values with Standard Deviations

	Emissions (mg/Nm^3)	
fuel assortment	SO_2	HCl
logging residues	<1[a]	<1[a]
logging residues + PA	<1[a]	6 ± 3
wheat straw-1	<1[a]	52 ± 4
wheat straw-1 + PA (low)	4 ± 2	62 ± 5
wheat straw-2 + PA (low)	8 ± 3	217 ± 29
wheat straw-2 + PA (medium)	23 ± 6	245 ± 30
wheat straw-2 + PA (high)	160 ± 20	246 ± 31

[a]Below detection level.

3.2. Particle Matter (PM) Mass Concentration and Size Distribution. Duplicated impactor measurements with a time separation of ∼2 h were performed for (i) pure logging residues and the assortment with PA, (ii) pure wheat straw-1 and the assortment with PA (low), and (iii) wheat straw-2 + PA (low and medium). For wheat straw-2 + PA (high), only one impactor measurement could be performed, because of total bed defluidization during the combustion period. The results from the impactor measurements are shown in Figures 2 and 3.

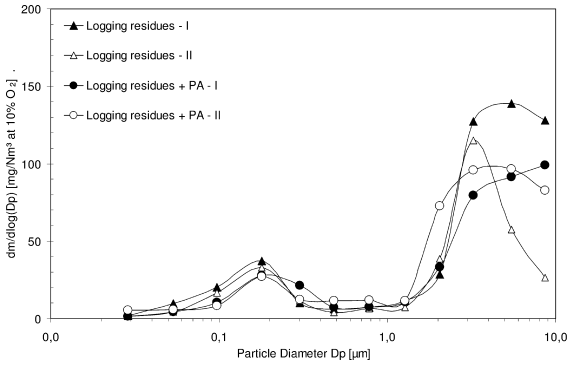

Figure 2. Particle mass size distribution in the flue gases during combustion of logging residues and the assortment with phosphoric acid (PA). Replicates of the impactor measurement are indicated with the suffixes -I and -II, respectively.

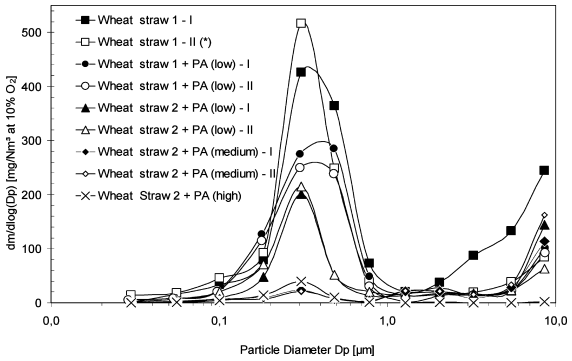

Figure 3. Particle mass size distribution in the flue gases during combustion of wheat straw assortments with phosphoric acid (PA). Wheat straw-1-II (*)[31] was sampled using the same experimental setup and analogous conditions, with the exception that the bed material was olivine instead of quartz. Replicates of the impactor measurement are indicated with the suffixes -I and -II, respectively.

Slightly lower concentrations of fine particles were observed for the logging residues containing PA, in comparison to the pure logging residues assortment. In both cases, the PM emissions were dominated by coarse ash particles (>1 μm; see Figure 2).

For all wheat straws assortments, the particle emissions between 0.03 μm and 10 μm were, in all cases, dominated by fine (<1 μm) particles. Significant reductions in fine particle mass concentrations were obtained for all wheat straw assortments with an increasing proportion of PA additive (see Figure 3).

Figure 4 shows the amount of coarse ash particles trapped in the cyclone separator (cut size >10 μm) given in mg/Nm^3 at 10% O_2. All calculations were made based on a fuel feeding rate of 0.6 kg/h for all fuels, and a flue gas rate of 80 NL/min. As can be seen from Figure 4, the amount of coarse ash particles formed during combustion is significantly affected by the addition of phosphorus.

3.3. Deposit Build-up Rate. The deposit build-up rates of the deposition probe are shown in Table 3. Generally, the build-up rate decreased with PA addition for both fuels, with the exception of wheat straw−1 + PA (low).

3.4. Chemical Composition of the Coarse and Fine Ash Particles. *3.4.1. SEM-EDS Analysis.* The results from SEM-EDS analyses of the coarse ash fractions (i.e., bed ash, cyclone ash, deposits on probe wind-side) and fine ash fractions (i.e., deposits on probe lee-side and impactor fine mode) are given in Figures 5−7, 9, and 10. The amount of deposits on the wind-side in the test with wheat straw-1 was too scarce to permit SEM-EDS and XRD analyses.

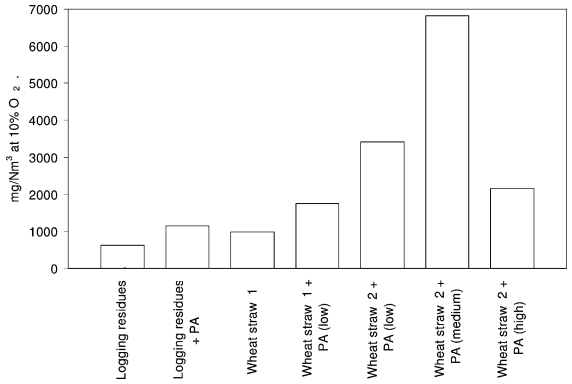

Figure 4. Total mass concentration of coarse ash particle emissions (>10 μm) trapped in the cyclone separator, given in units of mg/Nm^3 at 10% O_2, for all studied fuels/fuel assortments.

Table 3. Deposit Build-up Rates of the Deposition Probe

fuel/fuel assortment	deposit build-up rates (mg/(cm^2 h))
logging residues	0.14
logging residues + PA	0.08
wheat straw-1	0.34
wheat straw-1 + PA (low)	0.38
wheat straw-2 + PA (low)	0.32
wheat straw-2 + PA (medium)	0.15
wheat straw-2 + PA (high)	*a*

[a]Bed agglomeration after a 3-h experimental run.

For pure logging residue and wheat straws, the coarse ash fractions were found to have, in principle, similar elemental compositions, dominated by K, Ca, and Si, although with different K/Ca ratios (see Figures 5−7). Furthermore, as clearly shown, the PA addition resulted in an increase in phosphorus content.

The cyclone ash particles were analyzed more in detail. Supplementary SEM-EDS spot analyses were carried out on the samples in order to study the interaction between the fuel ash and the PA additive. Figure 8 shows SEM pictures of typical cyclone ash particles for pure logging residues and the assortment with PA, pure wheat straw-1, and wheat straw-2 + PA (low, medium, and high) assortments. The elemental composition of each ash cyclone particle marked in Figure 8 is given in Tables 4 and 5.

Pure logging residues cyclone ash was mostly dominated by Ca- and Si-rich particles. For the assortment with PA, ash aggregates of different sizes were found. The SEM-EDS analysis revealed the formation of spherical ash particles with a smooth surface and a composition dominated by P, K, Ca, Mg, and Si (see Figures 8a and 8b, and Table 4). Pure wheat straw-1 cyclone ash was mostly dominated by particles rich in silicon and potassium, and the assortment with PA revealed the formation of P-rich ash aggregates, but abundance of Si- and K-rich particles were still found. For wheat straw-2 + PA (low and medium) assortments, SEM-EDS analysis revealed the formation of ash aggregates of different sizes, mainly formed by crystalline structures with a composition dominated by P, K,

dx.doi.org/10.1021/ef300275e | *Energy Fuels* 2012, 26, 3012−3023

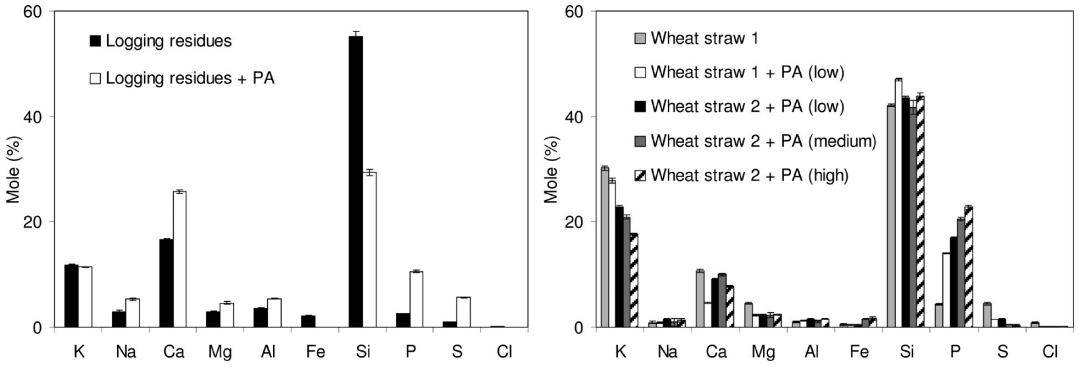

Figure 5. Elemental compositions on a carbon-free and oxygen-free basis of the bed ash particles during combustion of the logging residues (left) and wheat straw (right) assortments.

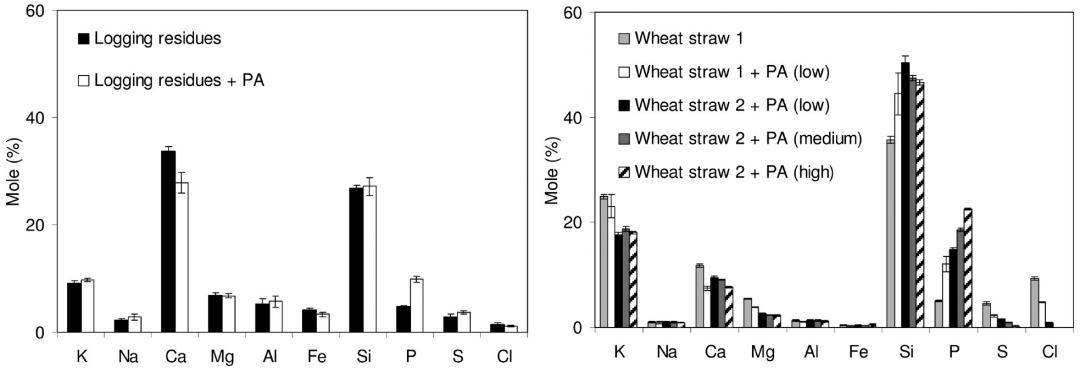

Figure 6. Elemental compositions on a carbon-free and oxygen-free basis of the cyclone separator ash particles (>10 μm), during combustion of the logging residues (left) and wheat straw (right) assortments.

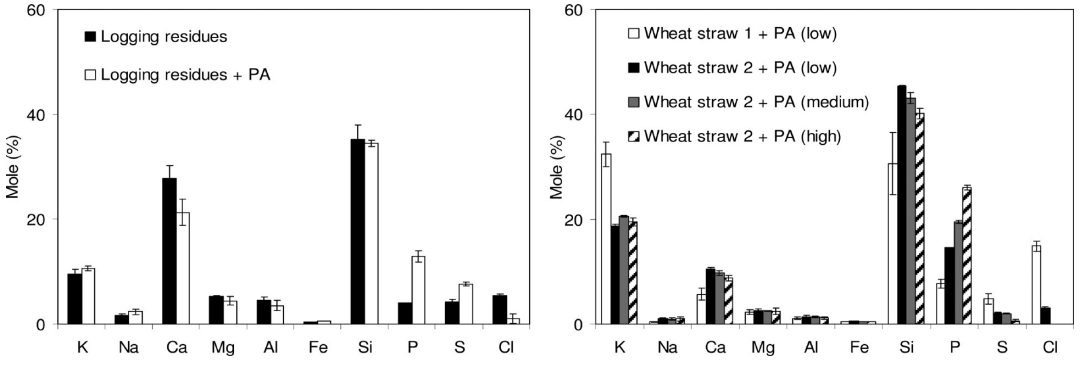

Figure 7. Elemental compositions on a carbon-free and oxygen-free basis of the deposition probe wind-side sampled at a temperature of 450 °C, during combustion of the logging residues (left) and wheat straw (right) assortments.

Ca, and Si (see Figures 8d and 8e, and Table 5). For the wheat straw-2 + PA (high) assortment, SEM-EDS analysis showed the formation of spherical ash particles with a smooth surface and a composition dominated by P, K and minor amounts of Si, and ash aggregates rich in P, K, Si, and Ca (see Figure 8f, and Table 5).

The amount of deposits on the lee-side in the test with wheat straw-2 + PA (high) was too scarce to permit SEM-EDS and XRD analyses. All assortments of logging residues and wheat straws with the PA additive gave lee-side deposits with increased content of phosphorus and sulfur, and decreased content of chlorine, when compared to the pure fuels. Wheat straw-2 + PA (medium) assortment lee-side deposits were free of chlorine, as seen in Figure 9.

Fine particles were dominated by potassium, chlorine, and sulfur for pure logging residues and wheat straw-1. A general observation when increasing the phosphorus in the fuel by using the PA additive is that the fine particles composition changed from a system dominated by potassium and chlorine to one dominated by potassium and sulfur. Wheat straw-2 + PA (high) fine particles were rich in potassium, sulfur, and phosphorus, with no chlorine detected, as seen in Figure 10.

3.4.2. Powder XRD Analysis. In Tables 6 and 7, the results from the P-XRD analyses of formed crystalline coarse ash fractions (given as BA, CA, DPW, and ICM), and fine ash fractions (given as IFM and DPL) are shown. Note that the coarse ash fractions include material that may have been partially molten and, upon cooling, formed crystalline and amorphous materials,

dx.doi.org/10.1021/ef300275e | *Energy Fuels* 2012, 26, 3012–3023

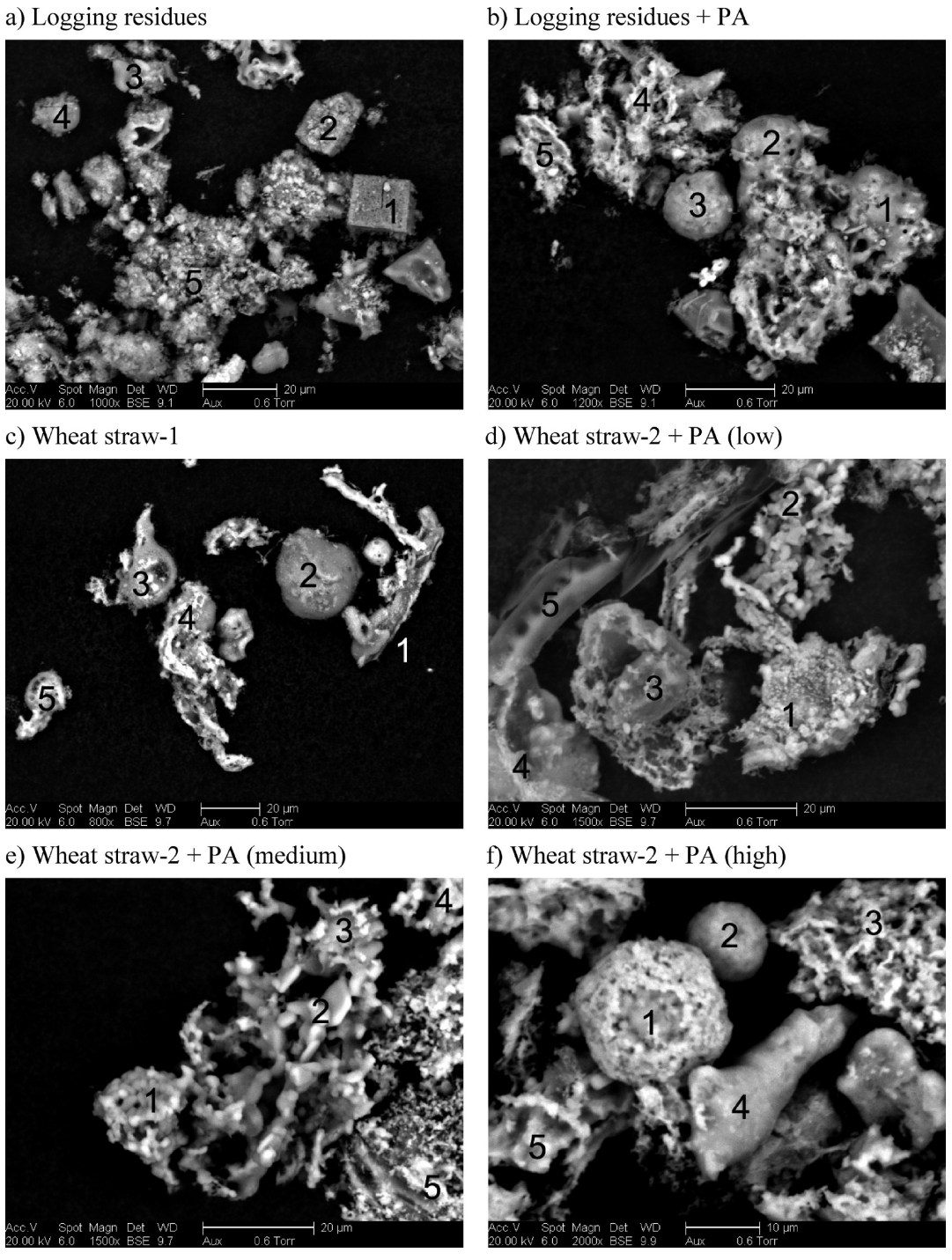

Figure 8. Scanning electron microscopy (SEM) images of typical cyclone ash particles formed during combustion of logging residues and the assortment with PA, wheat straw-1 and wheat straw-2 + PA (low, medium, and high) assortments.

where the latter cannot be directly identified by P-XRD analysis.

The crystalline material in the coarse ash fractions from pure logging residues was dominated by alkali-earth oxides, carbonates, and silicates. In combustion with this fuel, the phosphorus is found in the coarse ash fraction as apatite. For pure wheat straw-1, the crystalline phases in the coarse ash fractions were dominated by of K-sulfates, K-chlorides, Ca-phosphates, and Ca−K-phosphates. Fine particles were found in the tests with both fuels dominated by K-chlorides and K-sulfates.

The addition of phosphorus (as PA) to logging residues and both wheat straws (wheat straw-1 and -2) resulted in a coarse ash fraction with increased content of Ca−K-phosphates and K−Mg-phosphates, compared to the tests with pure fuels. Furthermore, PA addition resulted in an increased of cristobalite (SiO_2) in the coarse ash for all wheat straw assortments. Fine particles were dominated by K-sulfates instead of K-chlorides, as was the case for the pure logging residue and wheat straw fuels.

3.4.3. Fraction of Potassium and Chlorine Found in Fine Particles (<1 μm). The fraction of potassium volatilized from

dx.doi.org/10.1021/ef300275e | *Energy Fuels* 2012, 26, 3012−3023

Table 4. Results from the SEM-EDS Spot Analyses Referring to Figures 8a and 8b

	Concentration (mol %)									
	Logging Residues					Logging Residues + PA				
element	1	2	3	4	5	1	2	3	4	5
K	1.7	2.8	10.9	8.7	6.4	10.0	21.3	23.3	22.0	26.7
Na	1.2	1.5	4.0	3.1	1.3	3.1	5.6	4.7	7.8	6.6
Ca	91.2	74.9	26.6	16.9	44.4	20.4	21.6	23.2	19.7	19.7
Mg	1.4	3.9	8.6	5.9	16.8	5.1	6.7	4.3	8.5	6.3
Al	0.5	2.1	0.9	2.1	1.9	5.9	7.3	5.1	4.8	4.8
Fe	0.1	0.8	0.8	0.5	0.6	1.1	1.6	0.6	0.6	1.0
Si	1.3	6.7	40.2	58.4	17.5	32.8	11.4	9.3	5.4	5.0
P	0.5	2.5	5.2	3.4	5.3	20.8	23.6	28.8	27.5	29.0
S	1.5	3.8	2.3	0.9	5.2	0.5	0.6	0.6	3.5	0.6
Cl	0.6	1.0	0.5	0.1	0.6	0.3	0.3	0.1	0.2	0.3

the bed during combustion that contributed to the formation of condensed deposits and fine particle matter (<1 μm) was estimated by the ratio between the calculated total amount of potassium found in fine particles (given by SEM-EDS analyses on impactor stages 4, 5, and occasionally 6) and the total fine particulate mass concentration in flue gases obtained from the impactor data), and the total amount of K introduced by the in-going fuel during the impactor sampling period, as shown in Figure 11. The results show a significant decrease in the degree of volatilization of K-species during combustion for all experiments where phosphoric acid was used as an additive. The fraction of chlorine found as fine particulate alkali chlorides is shown in Figure 12. For the wheat straw and for the assortment with low PA addition (P/K = 0.5), ~20% of the chlorine was estimated to form HCl. For higher phosphorus addition (P/K > 1.1), close to 100% of the chlorine was estimated to form HCl(g). In the latter cases, only small amounts of chlorine were found in the ash fractions.

4. DISCUSSION

It is well-established today that, during biomass combustion, fine-mode (<1 μm) ash particles are formed by condensation/nucleation of volatilized species during cooling of the flue gases, mainly consisting of alkali salts. During combustion, the potassium and sodium are released from the fuel particle/bed as gaseous hydroxides/chlorides, which by further reaction with sulfur (present as SO_2/SO_3) form K/Na-sulfates.[32−35] Coarse-mode (>1 μm) ash particles are usually formed by the coalescence and agglomeration of nonvolatile compounds formed during the char burnout, entrained from the fuel/sand bed to the flue gases.[36]

As a consequence of the addition of phosphorus to P-poor fuels, the composition of the fine-mode ash particles will be affected. The formation of alkali phosphates in the bed ash results in smaller amounts of alkali in the flue gases. This will generally affect the formation of K/Na-chlorides first, since sulfates are thermodynamically more stable than chlorides under conditions relevant for this study. Therefore, the proportion of alkali sulfates in the fine particulate emissions and HCl emissions will increase as a result of the phosphorus addition. The formation of the alkali sulfates will only be affected when the amount of phosphorus available for reaction in the combustion atmosphere is high enough to react with most of the volatile alkali metals in the fuel/fuel mixture, with a subsequent increase in the SO_2/SO_3 emissions.[37]

For logging residues, the ash transformation is governed by the relatively low potassium content and high calcium content in the fuel. Thus, for the pure fuel, the coarse ash fractions were dominated by alkali-earth oxides, carbonates, and silicates. The observed fine particulate matter was composed of KCl and K_2SO_4, which is consistent with previous studies.[36,38] When adding PA to this fuel, a slight reduction of fine particles that were rich in potassium was achieved, corresponding to increased amounts of potassium found in the coarse ash fractions as K−Ca/Mg-phosphates (see Figures 8a and 8b, Tables 4 and 6). These observations were confirmed by the variations in the concentrations of HCl and SO_2 in the flue gases (Table 2). As discussed previously, a small amount of PA additive will accordingly reduce the amount of volatilized potassium (Figure 11) and change the composition of the fine particles from a chloride-dominated system to a sulfate-dominated system (Figure 12) and subsequently increase the levels of HCl emissions.

For wheat straw, the ash transformation is governed by the high potassium, silicon, calcium, and chlorine content. Straws are well-known problematic fuels that, upon combustion, cause problems such as corrosive deposits and a large amount of fine particulate matter of K-chlorides and K-sulfates. In accordance with previous works, the fine ash particulate fraction in this study consisted mainly of KCl and K_2SO_4. The coarse ash fractions were dominated by potassium and silicon, although not found as crystalline matter (see Figures 5−7 and Table 7). Increased phosphorus content in the wheat straw fuel by PA addition caused clear changes in the ash transformation (in general) and alkali distribution (in particular). For the wheat straw-1 + PA and wheat straw-2 + PA (low and medium) fuel assortments, the qualitative effect of PA addition was similar, although with quantitative differences. However, for wheat straw-2 + PA (high), significant and interesting additional qualitative effects on ash transformation chemistry were found and, therefore, discussed separately. As shown in Table 7, the proportion of Ca−K-phosphates in coarse ash fractions was increased substantially, compared to the case with pure wheat straw, in parallel with the lower content of KCl in fine ash fractions. It is notable that, in the case of wheat straw-2 + PA (medium), almost no potassium was available for the formation of chlorides. Our interpretation is that the K-capturing effect of the PA additive resulted in lower concentration of K in the gas phase available for the formation of other salts. Furthermore, as a consequence of increased P content, Ca−K-phosphates and cristobalite (SiO_2) in coarse ash fractions were formed instead of potassium-rich silicates (see Figures 8c−e, Tables 5 and 7).

dx.doi.org/10.1021/ef300275e | Energy Fuels 2012, 26, 3012−3023

Table 5. Results from the SEM-EDS Spot Analyses Referring to Figures 8c–f

	Concentration (mol %)																			
	Wheat straw-1					Wheat straw-2 + PA (low)					Wheat straw-2 + PA (medium)					Wheat straw-2 + PA (high)				
element	1	2	3	4	5	1	2	3	4	5	1	2	3	4	5	1	2	3	4	5
K	36.7	23.6	23.4	26.2	23.4	38.2	36.1	25.5	28.2	1.4	34.8	30.6	34.3	21.7	13.4	40.5	37.0	30.2	32.9	29.0
Na	0.2	0.9	1.2	1.0	1.3	1.0	1.1	1.6	1.4	0.4	1.3	1.0	1.0	1.9	1.0	3.7	2.2	4.1	0.0	2.8
Ca	14.6	7.5	15.8	7.7	10.9	10.5	11.5	6.7	9.5	0.4	16.0	14.0	14.5	8.9	22.2	5.3	6.9	11.0	14.9	10.6
Mg	2.7	2.2	5.9	3.5	5.1	4.7	7.9	8.3	2.5	0.1	1.7	1.5	1.6	2.4	3.6	1.5	4.1	3.3	3.7	5.9
Al	0.9	0.6	0.1	1.0	1.0	0.8	0.2	0.5	0.2	0.1	0.9	0.4	0.0	0.4	0.9	0.7	0.3	0.8	0.0	1.4
Fe	0.2	0.0	0.4	0.4	0.2	0.1	0.3	0.9	0.5	0.2	0.2	0.3	0.1	0.1	0.1	0.4	0.1	0.4	0.5	0.3
Si	41.5	52.0	39.2	51.4	51.5	10.3	11.2	32.8	31.5	95.5	11.0	20.0	14.1	39.1	36.4	7.0	17.2	17.8	14.3	19.0
P	0.7	1.1	6.8	2.3	4.3	32.3	30.4	21.2	25.1	1.3	33.0	31.4	33.8	24.8	20.5	38.8	31.3	30.9	32.8	30.0
S	0.9	2.7	2.4	1.6	0.9	1.3	0.5	0.7	0.5	0.4	1.0	0.6	0.5	0.6	1.5	0.9	0.8	1.2	0.5	0.6
Cl	1.6	9.4	4.8	4.9	1.4	0.8	0.8	1.8	0.6	0.2	0.1	0.2	0.1	0.1	0.4	1.2	0.1	0.3	0.4	0.4

This presumably shows that the amount of potassium in the gas phase available for reaction with silica to form K-silicates is reduced by the addition of phosphorus. Generally, the levels of HCl and SO_2 in the flue gases from the assortments with PA additive were substantially higher than for the pure fuel, and increased with increasing proportion of P in the fuels (Table 2). That is, with higher levels of P introduced with the fuel, a lower amount of volatilized potassium is obtained, which resulted in a higher concentration of acidic gases in the emissions.

Increasing the phosphorus content even further in wheat straw (i.e., wheat straw-2 + PA (high)) leads to a clear additional effect on the behavior of K and P, illustrated by the presence of significant amounts of phosphorus in fine particles (Figure 10) and the determination of KPO_3 in the cyclone ash (Table 7). This effect is presumably explained by the formation of an ash composition limited to the K–P-rich part of the Ca–K–P system, where a region with a low eutectic temperature (590 °C) is formed between $K_5P_3O_{10}$ and KPO_3.[39−43] This points to the formation of an ash material in the bed section that probably was molten prior to cooling, explaining the short combustion time due to bed agglomeration in this assortment. An additional result of the presumed stickiness of the bed ash material was that the amount of "captured" coarse ash in the bed was significantly higher and the amount of entrained coarse cyclone ash particles was reduced (Figure 4), compared to the cases with lower PA addition. Generally speaking, based on the results from this case with high phosphorus content, it was obvious that the amount of calcium available for the formation of high-temperature-melting ternary phosphates, as discussed in previous studies,[22−25] was too low, resulting in significant amounts of volatile alkali-rich phosphates (see Figure 8f and Table 5). Furthermore, as shown in Table 2, this increased amount of volatilized phosphorus species reduces the chance for sulfur to react with gaseous potassium, to the extent that almost no sulfates were formed with high emissions of SO_2 as a result.

Accordingly, a general observation from this work, together with previous research in this field, is that the addition of phosphorus to these biomass fuels during FB combustion changes the alkali distribution from being dominated by amorphous K-silicate coarse ash fractions and fine particulate KCl, to a system dominated by crystalline coarse ash of K–Ca/Mg-phosphates and fine particulate K_2SO_4. In previous works on bed agglomeration, it was found that the coarse ash fractions were mainly composed by amorphous K-silicates, not detectable with XRD.[44,45] In the present work, this effect on the ash transformations is supported by the increasing coherence between the SEM-EDS and P-XRD analyses.

Furthermore, the work clearly illustrates that the molar relationship between alkali and alkaline-earth metals, i.e., (K + Na)/(Ca + Mg) is of vital importance when considering the influences of phosphorus on the ash transformation for the type of biomass fuels studied here. This implies that phosphorus should not be added to the extent that the formation of pure alkali phosphates is promoted, in excess of more stable ternary alkali–alkali-earth oxides–phosphates, since the formation of low-temperature phosphate melts potentially leads to increased bed agglomeration and fouling tendencies in fluidized-bed combustion. However, adding an insufficient amount of phosphorus implies only a limited alkali retention effect. With these conditions in mind, the largest amount of phosphorus that should be added to a fuel should preferably be restricted to the formation of $CaK_2P_2O_7$, which is a pyrophosphate that has been

determined to be the major ternary phosphate in this study. This compound has a reasonably high melting point, relative to the process temperatures used in fluidized-bed combustion technologies.

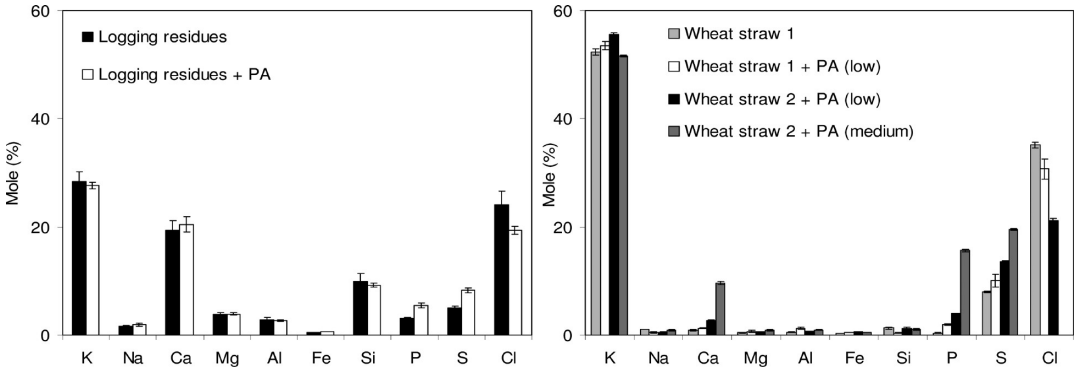

Figure 9. Elemental compositions on a carbon-free and oxygen-free basis of the deposition probe lee-side sampled at a temperature of 450 °C, during the combustion of the logging residues (left) and wheat straw (right) assortments.

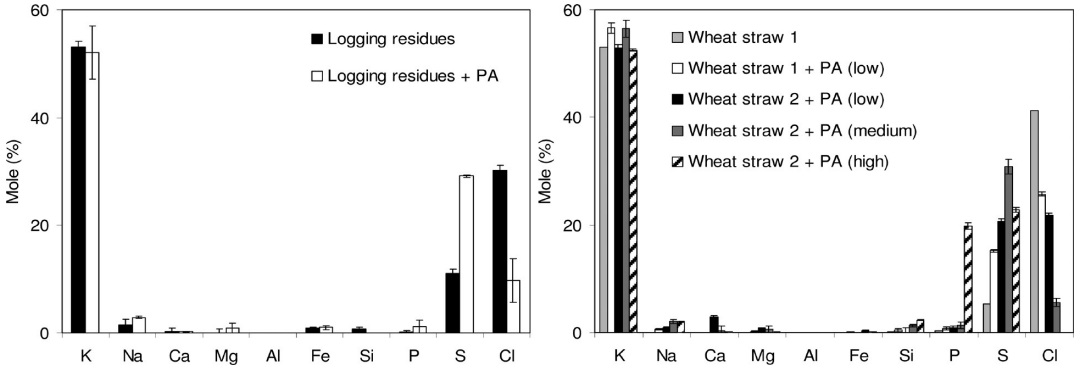

Figure 10. Elemental compositions on a carbon-, oxygen-, and aluminum-free basis of the fine particles (0.03−1 μm) sampled with the impactor during the combustion of the logging residues (left) and wheat straw (right) assortments.

Table 6. Crystalline Phases Identified with XRD in the Bed Ash Particles, Cyclone Ash, Impactor Fine/Coarse Mode, and Deposition Probe Lee/Wind Side for the Logging Residues Fuel Assortments[a]

	Logging Residues						Logging Residues + PA					
phase	BA	CA	IFM	ICM	DPL	DPW	BA	CA	IFM	ICM	DPL	DPW
SiO_2 (quartz)	70	19		2		22	5	16		4		25
$NaAlSi_3O_8$	7	12		1		20		16		9		15
$KAlSi_3O_8$	3	3		1				14		7		
CaO		7		7						5		
$CaCO_3$	2	28		6	9	23		21				19
MgO		2		11		3		3		3		3
$CaSO_4$		3		3	4	8	6	4		16	21	15
K_2SO_4	2	4	47	4	16				73	6	33	15
KCl		2	53	3	69	8		2	27	2	42	
$Ca_5(PO_4)_3(OH)$	5	12		28		6		7		19		6
$Ca_3(PO_4)_2$							33	6				
$CaMgP_2O_7$							17					
$CaKPO_4$											4	
$KMgPO_4$							12					
$CaK_2P_2O_7$							6	4				
$Ca_3Mg(SiO_4)_2$		8		23		7	12	7		14		2
$Ca_2MgSi_2O_7$						3	6					
$MgSiO_3$				10						6		
$CaMg(SiO_3)_2$	7									10		
SiO_2 (cristobalite)	4						3					

[a]Abbreviations used: BA, bed ash; CA, cyclone ash (>10 μm); IFM, impactor fine mode (<1 μm) ash particles; ICM, impactor coarse mode (1−10 μm) ash particles; DPL, deposition probe lee-side; and DPW, deposition probe wind side. The values in the table give the contents of crystalline phases (wt %) in the different samples as the result of semiquantitative refinement of the XRD data with Rietveld technique.

dx.doi.org/10.1021/ef300275e | Energy Fuels 2012, 26, 3012−3023

Table 7. Crystalline Phases Identified with XRD in the Bed Ash Particles, Cyclone Ash, Impactor Fine/Coarse Mode, and Deposition Probe Lee/Wind Side for the Wheat Straw Fuel Assortments[a,b]

	Wheat Straw-1						Wheat Straw-1 + PA (low)						Wheat Straw-2 + PA (low)						Wheat Straw-2 + PA (medium)						Wheat Straw-2 + PA (high)					
phase	BA	CA	IFM	ICM	DPL	DPW[b]	BA	CA	IFM	ICM	DPL	DPW	BA	CA	IFM	ICM[b]	DPL	DPW	BA	CA	IFM	ICM[b]	DPL	DPW	BA	CA	IFM[b]	ICM[b]	DPL[b]	DPW
SiO_2 (quartz)		1				n/a	51						10	5		n/a		10	3	3		n/a	1	10	5	6	n/a	n/a	n/a	7
$NaAlSi_3O_8$						n/a							5			n/a		20	6			n/a					n/a	n/a	n/a	
$KAlSi_3O_8$						n/a										n/a						n/a					n/a	n/a	n/a	
$CaCO_3$						n/a						3				n/a						n/a					n/a	n/a	n/a	
$CaSO_4$						n/a						2				n/a						n/a					n/a	n/a	n/a	
K_2SO_4	61	45	23	52	23	n/a	10	22	60	35	40	29	6	10	68	n/a	53	14			93	n/a	61	8			n/a	n/a	n/a	9
$K_3Na(SO_4)_2$	4			2	11	n/a				4		3				n/a						n/a					n/a	n/a	n/a	
KCl	3	35	77	22	65	n/a		17	40	18	55	30		3	32	v	37	3			7	n/a					n/a	n/a	n/a	
$Ca_5(PO_4)_3(OH)$	9	19		17		n/a										n/a						n/a			2		n/a	n/a	n/a	
$Ca_3(PO_4)_2$						n/a							1	12		n/a				10		n/a	9				n/a	n/a	n/a	
$CaKPO_4$	18					n/a	3	18		12						n/a						n/a					n/a	n/a	n/a	
$KMgPO_4$						n/a										n/a						n/a			9		n/a	n/a	n/a	
$CaK_2P_2O_7$						n/a	25	32		31	5	25	45	50		n/a	10	47	60	67		n/a	29	77	31	65	n/a	n/a	n/a	71
KPO_3						n/a										n/a						n/a				11	n/a	n/a	n/a	
$Ca_3Mg(SiO_4)_2$	2			7		n/a										n/a						n/a					n/a	n/a	n/a	
$Ca_2MgSi_2O_7$	3					n/a										n/a						n/a					n/a	n/a	n/a	
SiO_2 (cristobalite)						n/a	11	11				8	33	21		n/a		6	31	21		n/a		5	53	18	n/a	n/a	n/a	13

[a]Abbreviations used: BA, bed ash; CA, cyclone ash (>10 μm); IFM, impactor fine mode (<1 μm) ash particles; ICM, impactor coarse mode (1−10 μm) ash particles; DPL, deposition probe lee-side; and DPW, deposition probe wind side. The values in the table give the contents of crystalline phases (wt %) in the different samples as the result of semiquantitative refinement of the XRD data with Rietveld technique. [b]No data available, because of the scarce amount of sample.

dx.doi.org/10.1021/ef300275e | Energy Fuels 2012, 26, 3012−3023

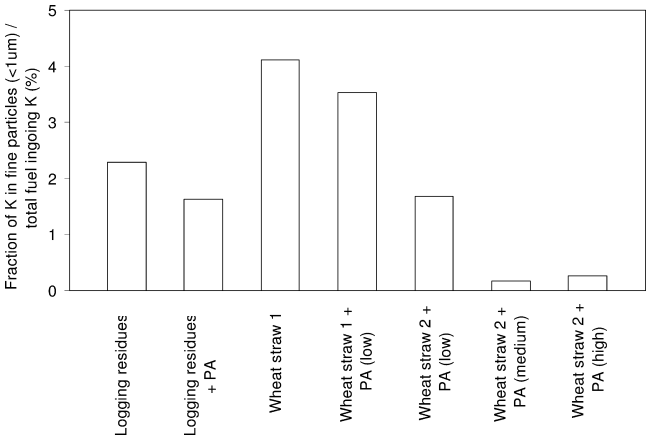

Figure 11. Fractions of the total amounts of potassium introduced with the in-going fuel that was found in fine particle matter (<1 μm) for the studied fuel assortments.

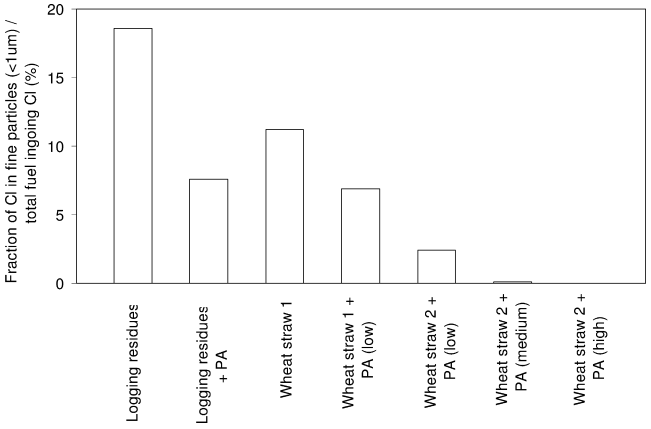

Figure 12. Fractions of total amounts of chlorine introduced with the in-going fuel that was found in fine particle matter (<1 μm) for the studied fuel assortments.

Finally, fluidized beds are particularly suitable for adding phosphorus to a fuel in order to reduce condensed deposits and fine particulate forming matter, because of a long fuel residence time and moderate process temperatures, compared to powder and grate applications. The combustion of phosphorus-rich fuels in powder-fired systems has proved to be problematic.[46] Thus, corrosion in superheaters and fouling problems caused by deposits rich in alkali metals and chlorine can be potentially reduced by employing fuel assortments/mixtures with a suitable molar balance between phosphorus on the one hand and potassium, sodium, calcium, and magnesium on the other hand, with the reservation that higher concentrations of acidic gases can be tolerated.

5. CONCLUSIONS

- A significant reduction of volatilized deposit and fine particle forming matter containing KCl as the main component was achieved by increasing the phosphorus content in the fuels.
- As a consequence, an increased amount of potassium was found in the coarse ash particle fractions, principally as $KMgPO_4$, $CaK_2P_2O_7$, $CaKPO_4$, and KPO_3, while the levels of HCl and SO_2 in the flue gases increased.
- Thus, a clear qualitative and quantitative effect of the addition of phosphorus on alkali distribution for both biomass fuels studied was found. The alkali distribution was changed from being dominated by amorphous K-silicate coarse ash fractions and fine particulate KCl to a system dominated by crystalline coarse ash of K−Ca/Mg-phosphates and fine particulate K_2SO_4.
- The phosphorus content in the fuel should not be increased to an extent where the formation of alkali-rich low-temperature-melting phosphates is promoted, since this increases the risk of both bed agglomeration as well as the release of alkali and phosphorus from the bed, which increases deposit and fine particle formation.

AUTHOR INFORMATION

Corresponding Author

*Tel.: +46 (0) 73 0491977. E-mail: Alejandro.Grimm@ltu.se.

Notes

The authors declare no competing financial interest.

ACKNOWLEDGMENTS

Financial support from the Swedish Research Council (VR) and the National (Swedish) Strategic Research Program Bio4Energy is gratefully acknowledged. The technical support given by Ulf Nordström (Energy Technology and Thermal Process Chemistry, Umeå University), during the experiments is gratefully appreciated.

REFERENCES

(1) Monti, A.; Di Virgilio, N.; Venturi, G. *Biomass Bioenergy* **2008**, *32*, 216−223.
(2) Ergudenler, A.; Ghaly, A. E. *Biomass Bioenergy* **1993**, *4*, 135−147.
(3) Nielsen, H. P.; Frandsen, F. J.; Dam-Johansen, K.; Baxter, L. L. *Prog. Energy Combust. Sci.* **2000**, 283−298.
(4) Miles, T. R.; Miles, T. R., Jr.; Baxter, L. L.; Bryers, R. W.; Jenkins, B. M.; Oden, L. L. *Biomass Bioenergy* **1996**, *10*, 125−138.
(5) Lundholm, K.; Nordin, A.; Öhman, M.; Boström, D. *Energy Fuels* **2005**, *19*, 2273−2278.
(6) Lundmark, D.; Mueller, C.; Backman, R.; Zevenhoven, M.; Skrifvars, B. J.; Hupa, M. *J. Energy Resourc. Technol.−Trans. ASME* **2010**, *132*, Article 031003.
(7) Pommer, L.; Öhman, M.; Boström, D.; Burvall, J.; Backman, R.; Olofsson, I.; Nordin, A. *Energy Fuels* **2009**, *23*, 4245−4253.
(8) Aho, M.; Ferrer, E. *Fuel* **2005**, *84*, 201−212.
(9) Baxter, L. *Fuel* **2005**, *84*, 1295−1302.
(10) Åmand, L. E.; Leckner, B.; Eskilsson, D.; Tullin, C. *Fuel* **2006**, *85*, 1313−1322.
(11) Elled, A. L.; Davidsson, K. O.; Åmand, L. E. *Biomass Bioenergy* **2010**, *34*, 1546−1554.
(12) Aho, M.; Yrjas, P.; Taipale, R.; Hupa, M.; Silvennoinen, J. *Fuel* **2010**, *89*, 2376−2386.
(13) Iisa, K.; Lu, Y.; Salmenoja, K. *Energy Fuels* **1999**, *13*, 1184−1190.
(14) Viklund, P.; Pettersson, R.; Hjörnhede, A.; Henderson, P.; Sjövall, P. *Corros. Eng. Sci. Technol.* **2009**, *44*, 234−240.
(15) Tran, K. Q.; Steenari, B. M.; Iisa, K.; Lindqvist, O. *Energy Fuels* **2004**, *18*, 1870−1876.
(16) Steenari, B. M.; Lindqvist, O. *Biomass Bioenergy* **1998**, *14*, 67−76.
(17) Coda, B.; Aho, M.; Berger, R.; Heing, K. R. G. *Energy Fuels* **2001**, *15*, 680−690.
(18) Turn, S. Q.; Kinoshita, C. M.; Ishimura, D. M.; Zhou, J.; Hiraki, T. T.; Masutani, S. M. *J. Inst. Energy* **1998**, *71*, 163−177.
(19) Aho, M. *Fuel* **2001**, *80*, 1943−1951.
(20) Henderson, P.; Szakálos, P.; Pettersson, R.; Andersson, C.; Högberg, J. *Mater. Corros.* **2006**, *57*, 128−134.

(21) Öhman, M.; Nordin, A.; Lundholm, K.; Boström, D.; Hedman, H.; Lundberg, M. *Energy Fuels* **2003**, *17*, 1153−1159.
(22) Boström, D.; Eriksson, G.; Boman, C.; Öhman, M. *Energy Fuels* **2009**, *23*, 2700−2706.
(23) Grimm, A.; Skoglund, N.; Boström, D.; Öhman, M. *Energy Fuels* **2011**, *25*, 937−947.
(24) Boström, D.; Grimm, A.; Boman, C.; Björnbom, E.; Öhman, M. *Energy Fuels* **2009**, *23*, 5184−5190.
(25) Lindström, E.; Sandström, M.; Boström, D.; Öhman, M. *Energy Fuels* **2007**, *21*, 710−717.
(26) Wu, H.; Castro, M.; Jensen, P. A.; Frandsen, F. P.; Glarborg, P.; Dam-Johansen, K.; Røkke, M.; Lundtorp, K. *Energy Fuels* **2011**, *25*, 2874−2886.
(27) Beck, J.; Unterberger, S. *Fuel* **2006**, *85*, 1541−1549.
(28) Novaković, A.; van Lith, S. C.; Frandsen, F. J.; Jensen, P. A.; Holgersen, L. B. *Energy Fuels* **2009**, *23*, 3423−3428.
(29) ICDD. *The Powder Diffraction File, PDF-2*; International Centre for Diffraction Data, Newtowne Square, PA, 2004.
(30) Inorganic Crystal Structure Database, ICSD. National Institute of Standards and Technology, Fachinformation Zentrum, Karlsruche, Germany.
(31) Grimm, A.; Boström, D.; Lindberg, T.; Fredriksson, A.; Öhman, M. Bed Agglomeration Characteristics during Fluidized Olivine Bed Combustion of Typical Biofuels. In *19th European Biomass Conference and Exhibition*, June 6−10, 2011, Berlin, Germany.
(32) Zeuthen, J. H.; Jensen, P. A.; Jensen, J. P.; Livbjerg, H. *Energy Fuels* **2007**, *21*, 699−709.
(33) Hindiyarti, L.; Frandsen, F.; Livbjerg, H.; Glarborg, P.; Marshall, P. *Fuel* **2008**, *87*, 1591−1600.
(34) Christensen, K. A.; Stenholm, M.; Livbjerg, H. *J. Aerosol Sci.* **1998**, *29*, 421−444.
(35) Knudsen, J. N.; Jensen, P. A.; Dam-Johansen, K. *Energy Fuels* **2004**, *18*, 1385−1399.
(36) Lind, T. T.; Valmari, E.; Kauppinen, K.; Nilsson, K.; Sfiris, G.; Maenhaut, W. *Proc. Combust. Inst.* **2000**, *28*, 2287−2295.
(37) Boström, D.; Skoglund, N.; Grimm, A.; Boman, C.; Öhman, M.; Broström, M.; Backman, R. *Energy Fuels* **2012**, *26*, 85−93.
(38) Pagels, J.; Strand, M.; Rissler, J.; Szpila, A.; Gudmundsson, A.; Bohgard, M.; Lillieblad, L.; Sanati, M.; Swietlicki, E. *J. Aerosol Sci.* **2003**, *34*, 1043−1059.
(39) Znamierowska, T. *Pol. J. Chem.* **1978**, *52* (6), 1127−1134.
(40) Znamierowska, T. *Pol. J. Chem.* **1979**, *53* (7−8), 1415−1423.
(41) Znamierowska, T. *Pol. J. Chem.* **1978**, *52* (10), 1889−1895.
(42) Znamierowska, T. *Pol. J. Chem.* **1981**, *55* (4), 747−756.
(43) Znamierowska-Kubicka, T. *Rocz. Chem.* **1977**, *51* (11), 2089−2098.
(44) Öhman, M.; Nordin, A.; Skrifvars, B. J.; Backman, R.; Hupa, M. *Energy Fuels* **2000**, *14*, 169−178.
(45) Lin, W.; Dam-Johansen, K.; Frandsen, F. *Chem. Eng. J.* **2003**, *96*, 171−185.
(46) Eriksson, G. *Residues from biochemical production of transport biofuels in Northern Europe: Combustion properties and applications*, Ph.D. Dissertation, Luleå University of Technology, Luleå, Sweden, 2009 (ISBN 978-91-7439-058-2).